

Measurement of the equivalent complex permittivity of electromagnetic structural materials without prior thickness

Xiang-Bao Zhu(朱香宝), Yun-Peng Zhang(张云鹏), Pin-Hong Xie(谢品鸿), Yi-Hang Tu(涂一航), Jia-Wei Long(龙嘉威), Xue Niu(牛雪), Chong Gao(高冲), Cheng-Yong Yu(余承勇), Yong Gao(高勇), and En Li(李恩)
Citation: Chin. Phys. B, 2026, 35 (**4**): 040101. DOI: 10.1088/1674-1056/ae0434
http://cpb.iphy.ac.cn; http://iopscience.iop.org/cpb

What follows is a list of articles you may be interested in

Effect of water vapor on the structure and stability of self-organized patterns in atmospheric-pressure pulsed radio-frequency dielectric barrier discharges

Man-Qiang Du(杜满强), Wen-Fu Wei(魏文赋), Zhen-Feng Ding(丁振峰), Liang-Wen Qi(漆亮文), Xiao-Dong Wen(温晓东), and Bin Sun(孙斌)
Chin. Phys. B, 2026, 35 (**3**): 035201. DOI: 10.1088/1674-1056/adf181

Simulation on atmospheric pressure barrier discharge with varying relative position between two wavy dielectric surfaces

Xue-Chen Li(李雪辰), Wen-Jie Wan(万文杰), Xiao-Qian Liu(刘晓倩), Mo Chen(陈墨), Kai-Yue Wu(吴凯玥), Jun-Xia Ran(冉俊霞), Xue-Xia Pang(庞学霞), Xue-Xue Zhang(张雪雪), Jia-Cun Wu(武珈存), Peng-Ying Jia(贾鹏英), and Hui Sun(孙辉)
Chin. Phys. B, 2025, 34 (**3**): 035202. DOI: 10.1088/1674-1056/ada43d

Application of the body of revolution finite-element method in a re-entrant cavity for fast and accurate dielectric parameter measurements

Tianqi Feng(冯天琦), Chengyong Yu(余承勇), En Li(李恩), and Yu Shi(石玉)
Chin. Phys. B, 2023, 32 (**3**): 030101. DOI: 10.1088/1674-1056/ac7f91

Attenuation characteristics of obliquely incident electromagnetic wave in weakly ionized dusty plasma based on modified Bhatnagar-Gross-Krook collision model

Zhaoying Wang(王召迎), Lixin Guo(郭立新), and Jiangting Li(李江挺)
Chin. Phys. B, 2021, 30 (**4**): 045203. DOI: 10.1088/1674-1056/abe230

Measurement of the equivalent complex permittivity of electromagnetic structural materials without prior thickness

Xiang-Bao Zhu(朱香宝)[1], Yun-Peng Zhang(张云鹏)[1,†], Pin-Hong Xie(谢品鸿)[1], Yi-Hang Tu(涂一航)[2], Jia-Wei Long(龙嘉威)[1], Xue Niu(牛雪)[1], Chong Gao(高冲)[1], Cheng-Yong Yu(余承勇)[1], Yong Gao(高勇)[3], and En Li(李恩)[1]

[1] *School of Electronic Science and Engineering, University of Electronic Science and Technology of China, Chengdu* 611731, *China*
[2] *School of Electronic Information and Electrical Engineering, Chengdu University, Chengdu* 610106, *China*
[3] *School of Computer Science and Information Engineering, Hefei University of Technology, Hefei* 230601, *China*

(Received 7 July 2025; revised manuscript received 13 August 2025; accepted manuscript online 8 September 2025)

Electromagnetic structural materials exhibit significant sensitivity to the polarization state and incidence angle of electromagnetic waves. The equivalent complex permittivity is the core parameter that describes the dielectric properties of electromagnetic structural materials. Therefore, accurate characterization of their equivalent complex permittivity is essential for establishing electromagnetic models and guiding the design of functional devices. This paper proposes a broadband inversion method based solely on reflection measurements at different incident polarizations and incident angles. By establishing a set of adaptive equations for multi-reflection measurement states under oblique incidence, the proposed method directly resolves the equivalent complex permittivity without requiring prior knowledge of the sample thickness and iterative phase unwrapping, and obtains broadband measurement results in a single measurement. The simulation and experimental results show that this method has good testing consistency and accuracy. This study provides a high-precision, low-cost and efficient testing solution for dielectric property evaluation of electromagnetic structural materials. It can simplify the complex modeling design of electromagnetic structural materials into an equivalent single-layer material design, providing a reference value for rapid analysis of the scattering characteristics of complex structures.

Keywords: equivalent complex permittivity, electromagnetic structural materials, broadband, thickness unknown

PACS: 01.40.gf, 52.25.Mq, 52.70.Gw

DOI: 10.1088/1674-1056/ae0434 **CSTR:** 32038.14.CPB.ae0434

1. Introduction

With the rapid development of electronic information technology, electromagnetic structural materials (EMSMs), such as honeycomb materials and porous dielectric materials, have attracted much attention in next-generation radome design, high-performance electromagnetic shielding, and radar detection[1–4] due to their unique electromagnetic properties (incident polarization selectivity and angular dependence). The complex permittivity serves as a core parameter to describe the electromagnetic characteristics of materials;[5] its precise extraction is a key prerequisite for optimizing material design and improving device performance.

When designing components based on EMSM, existing methods require modeling of complex microstructures with electrically small dimensions on electrically large components. This results in excessively long simulation or computation time under multi-scale grid partitioning and densely distributed periodic microstructures. More serious situations can lead to numerical solution failure. Therefore, extracting the equivalent permittivity of EMSM and mapping it to anisotropic single-layer materials can drastically shorten design cycles. This has significant value in simplifying the design of EMSM-based components.

There are many testing methods that can be used to measure the dielectric properties of materials, such as the rectangular waveguide method,[6,7] resonant cavity method,[8,9] coaxial method[10] and free-space method.[11–13] Among them, the free-space method has become the preferred method for testing EMSM under oblique incidence due to its unique advantages such as broadband, non-contact, non-destructive, multi-polarization and angle control.

The methods in Refs. [11–13] utilize the free-space method to obtain the complex permittivity of different materials; these methods have good test results under vertical incidence conditions. However, they did not consider test under different polarization states and incident angles. Although prior works[14,15] have demonstrated the feasibility of retrieving the equivalent complex permittivity of materials under oblique incidence, their reliance on precise knowledge of material thickness constitutes a fundamental limitation, precluding their application to scenarios involving unknown thickness. In addition, reflection parameters and transmission parameters are usually required for equivalent complex permittivity inversion.[16,17] However, it is difficult to obtain transmission parameters when samples cannot be accessed from

†Corresponding author. E-mail: zyp_ee@163.com

© 2026 Chinese Physical Society and IOP Publishing Ltd. All rights, including for text and data mining, AI training, and similar technologies, are reserved.

the back side. Finally, obtaining the equivalent complex permittivity of materials through the free-space method often introduces a multi-value problem due to phase ambiguity.[18,19] Although this problem can be solved by the improved NRW algorithm,[20] stepwise[21] and other methods, they also increase the complexity and uncertainty of the calculation.

In this paper, we propose a broadband dielectric inversion methodology for extracting the equivalent complex permittivity of EMSM under multi-polarization, multi-angle reflection configurations. This method establishes multiple equations to solve the equivalent complex permittivity of materials through multi-reflection test states under oblique incidence. It does not need to know the thickness of the sample and is a stable calculation method that avoids phase unwrapping. Furthermore, we establish a corresponding 8–12 GHz band testing system and verify the effectiveness and accuracy of the method through simulation and testing. This study provides valuable guidance for rapidly evaluating the dielectric properties of composite materials, greatly simplifying the simulation modeling process of complex structures.

2. Proposed methodology

2.1. Test model and reflection measurement theory

Figure 1 illustrates the oblique incidence model for characterizing the dielectric properties of the material under test (MUT). This model categorizes electromagnetic (EM) wave propagation characteristics into two fundamental polarization states: transverse electric (TE) polarization and transverse magnetic (TM) polarization, determined by the electric field orientation relative to the plane of incidence. Here, $\boldsymbol{E}_{\rm i}$ and $\boldsymbol{H}_{\rm i}$ are the electric and magnetic fields of the incident wave, $\boldsymbol{E}_{\rm r}$ and $\boldsymbol{H}_{\rm r}$ are the electric and magnetic fields of the reflected wave, and θ is the incident angle of the incident wave. Due to the sensitivity of EMSM to the angle and polarization of incident waves, it is essential to introduce the incident angle parameter in the process of extracting the equivalent complex permittivity.

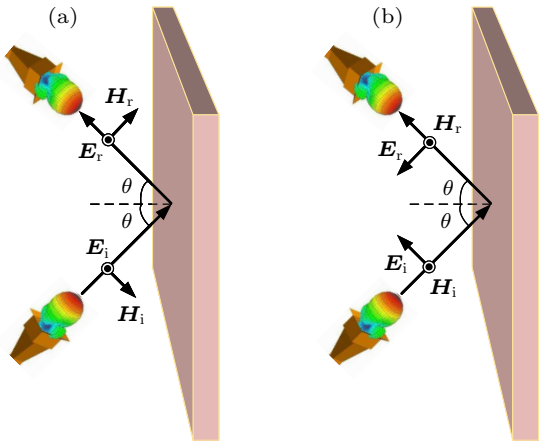


Fig. 1. Oblique incidence model. (a) TE polarization. (b) TM polarization.

The test for the reflection state can be simplified into the model shown in Fig. 2. As shown in Fig. 2(a), the entire antenna structure can be utilized as a waveguide to a free-space transmission line converter under vertical incidence. Port 1 is the measurement port and port 2 is the analog plane wave port.

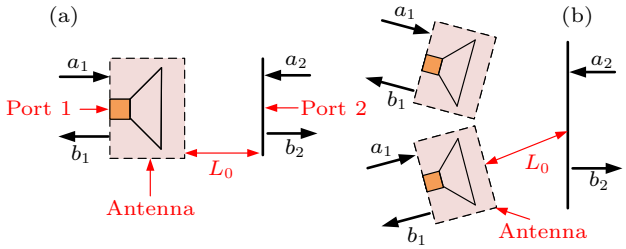


Fig. 2. Reflection equivalent model. (a) Vertical incidence single antenna model. (b) Separation model for transmitting and receiving antennas under oblique incidence.

If the incident and reflected waves at port 1 are a_1 and b_1, respectively, and the incident and reflected waves at port 2 are a_2 and b_2, respectively, this leads to

$$\begin{pmatrix} b_1 \\ b_2 \end{pmatrix} = \begin{pmatrix} S_{11} & S_{12} \\ S_{21} & S_{22} \end{pmatrix} \begin{pmatrix} a_1 \\ a_2 \end{pmatrix}. \tag{1}$$

Here, S_{11} and S_{22} represent the reflection coefficients of ports 1 and 2, respectively. S_{21} represents the transmission coefficient from port 1 to port 2, and S_{12} represents the transmission coefficient from port 2 to port 1.

If the reflection coefficient of the antenna is P, then $S_{11} = P$. Since port 2 is an analog plane wave port, $S_{22} = 0$. According to the principle of optical path reversibility, the antenna can be regarded as a heterogeneous device, so $S_{12} = S_{21} = T$, where T is the transmission coefficient of the antenna. Therefore, from formula (1),

$$b_1 = Pa_1 + Ta_2, \tag{2}$$

$$b_2 = Ta_1. \tag{3}$$

In addition, the reflection coefficient of port 1 is $P_1 = b_1/a_1$ and the reflection coefficient of port 2 is $P_2 = b_2/a_2$. By combining formulas (2) and (3), the reflection coefficient P_1 of port 1 is

$$P_1 = P + T \cdot T \cdot P_2. \tag{4}$$

When testing the reflection coefficient under oblique incidence states, it is necessary to separate the transmitting and receiving antennas, as shown in Fig. 2(b). If two antennas are assumed to be the same device, the conclusion of formula (4) can also be obtained.

2.2. Multi-state reflection measurement method

Based on the above testing model and reflection measurement theory, this paper proposes an equivalent complex permittivity testing method under multiple-reflection states. Figure 3 details four experimental setups that validate the multi-state measurement approach. Due to the separate placement of

the transmitting antenna and receiving antenna under oblique incidence, the reflection parameters in each test state are characterized by measuring the transmission parameters between the two antennas in Fig. 3.

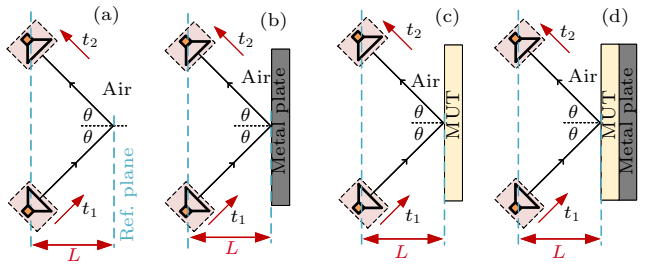


Fig. 3. The proposed four test states. (a) Test condition under air. (b) Test condition under a metal plate. (c) Test condition under the MUT. (d) Test condition under the MUT of the backing metal plate.

In Fig. 3(a), the two antennas are oriented towards free space, and P_{air} of the reflection coefficient measured in air can be expressed as[22]

$$P_{\text{air}} = P_0. \tag{5}$$

Here, P_0 accounts for the mutual coupling between the two antennas, and incorporates the effects of multiple reflections within the measurement system, including those arising from internal antenna structures and the surrounding test environment.

In Fig. 3(b), a metal plate is placed at a vertical distance of L from the two antennas. The plane on the side of the metal plate near the two antennas is designated as the reference plane. When the metal plate is placed, the reflection coefficient obtained by testing needs to be divided into two cases: TE polarization and TM polarization. $P_{\text{m}\perp}$ under TE polarized incident and $P_{\text{m}\parallel}$ under TM polarized incident are respectively represented as

$$P_{\text{m}\perp} = P_0 - t_1 t_2 \, \mathrm{e}^{-\mathrm{j}k_0 2L/\cos\theta}, \tag{6}$$

$$P_{\text{m}\parallel} = P_0 + t_1 t_2 \, \mathrm{e}^{-\mathrm{j}k_0 2L/\cos\theta}, \tag{7}$$

where t_1 and t_2 are the transmission and reception loss terms of the two antennas, respectively, and k_0 is the free-space wavenumber.

In Fig. 3(c), the metal plate is replaced by the MUT. The reflection coefficients $P_{\text{MUT}\perp}$ (TE polarization) and $P_{\text{MUT}\parallel}$ (TM polarization) obtained from testing with the MUT in this state are

$$P_{\text{MUT}\perp} = P_0 + t_1 t_2 \, \mathrm{e}^{-\mathrm{j}k_0 2L/\cos\theta} R_\perp \frac{1 - T_{\text{MUT}}^2}{1 - R_\perp^2 T_{\text{MUT}}^2}, \tag{8}$$

$$P_{\text{MUT}\parallel} = P_0 + t_1 t_2 \, \mathrm{e}^{-\mathrm{j}k_0 2L/\cos\theta} R_\parallel \frac{1 - T^2}{1 - R_\parallel^2 T^2}, \tag{9}$$

where T_{MUT} is the transmission coefficient inside the MUT, and $R_\perp$ and $R_\parallel$ are the reflection coefficients from air to the MUT under TE polarization and TM polarization incident waves, respectively. Their expressions are[23]

$$R_\perp = \frac{\cos\theta - \sqrt{\varepsilon_{\text{r}\perp} - \sin^2\theta}}{\cos\theta + \sqrt{\varepsilon_{\text{r}\perp} - \sin^2\theta}}, \tag{10}$$

$$R_\parallel = \frac{\varepsilon_{\text{r}\parallel}\cos\theta - \sqrt{\varepsilon_{\text{r}\parallel} - \sin^2\theta}}{\varepsilon_{\text{r}\parallel}\cos\theta + \sqrt{\varepsilon_{\text{r}\parallel} - \sin^2\theta}}, \tag{11}$$

where $\varepsilon_{\text{r}\perp}$ and $\varepsilon_{\text{r}\parallel}$ are the equivalent complex permittivities of the MUT under TE polarization and TM polarization, respectively, and θ is the incident angle of the incident EM wave.

In Fig. 3(d), the metal plate is placed adjacent to the back of the MUT based on the test state in Fig. 3(c). The reflection coefficients $P_{\text{MM}\perp}$ (TE polarization) and $P_{\text{MM}\parallel}$ (TM polarization) obtained from testing with both the MUT and the metal plate placed simultaneously are

$$P_{\text{MM}\perp} = P_0 + t_1 t_2 \, \mathrm{e}^{-\mathrm{j}k_0 2L/\cos\theta} \frac{R_\perp - T_{\text{MUT}}^2}{1 - R_\perp T_{\text{MUT}}^2}, \tag{12}$$

$$P_{\text{MM}\parallel} = P_0 + t_1 t_2 \, \mathrm{e}^{-\mathrm{j}k_0 2L/\cos\theta} \frac{R_\parallel + T_{\text{MUT}}^2}{1 + R_\parallel T_{\text{MUT}}^2}. \tag{13}$$

By completing all the testing steps through the four testing states mentioned above, combining formulas (5)–(9) and (12)–(13) yields the following results:

$$P_{1\perp} = \frac{P_{\text{MUT}\perp} - P_{\text{air}}}{P_{\text{air}} - P_{\text{m}\perp}} = \frac{R_\perp\left(1 - T_{\text{MUT}}^2\right)}{1 - R_\perp^2 T_{\text{MUT}}^2}, \tag{14}$$

$$P_{2\perp} = \frac{P_{\text{MM}\perp} - P_{\text{air}}}{P_{\text{air}} - P_{\text{m}\perp}} = \frac{R_\perp - T_{\text{MUT}}^2}{1 - R_\perp T_{\text{MUT}}^2}, \tag{15}$$

$$P_{1\parallel} = \frac{P_{\text{MUT}\parallel} - P_{\text{air}}}{P_{\text{m}\parallel} - P_{\text{air}}} = \frac{R_\parallel\left(1 - T_{\text{MUT}}^2\right)}{1 - R_\parallel^2 T_{\text{MUT}}^2}, \tag{16}$$

$$P_{2\parallel} = \frac{P_{\text{MM}\parallel} - P_{\text{air}}}{P_{\text{m}\parallel} - P_{\text{air}}} = \frac{R_\parallel + T_{\text{MUT}}^2}{1 + R_\parallel T_{\text{MUT}}^2}. \tag{17}$$

According to formulas (14)–(17), $R_\perp$ and $R_\parallel$ can be calculated as follows:

$$\begin{aligned} R_\perp &= -\xi_\perp \pm \sqrt{\xi_\perp^2 - 1}, \\ \xi_\perp &= \frac{(P_{1\perp} - 1) - (P_{1\perp} + 1)P_{2\perp}}{2P_{1\perp}}, \\ R_\parallel &= \frac{-\xi_\parallel \pm \sqrt{\xi_\parallel^2 - 4P_{1\parallel}^2}}{2P_{1\parallel}}, \end{aligned} \tag{18}$$

$$\xi_\parallel = (P_{2\parallel} - P_{1\parallel} - P_{1\parallel}P_{2\parallel} - 1). \tag{19}$$

In order to simplify formulas (18) and (19), symbols $\xi_\perp$ and $\xi_\parallel$ without special physical meaning were introduced.

Their unique correct values can be determined by $|R_\perp| \leq 1$ and $|R_\parallel| \leq 1$. Finally, through formulas (10) and (11), $\varepsilon_{\text{r}\perp}$ and $\varepsilon_{\text{r}\parallel}$ are obtained as follows:

$$\varepsilon_{\text{r}\perp} = \frac{\cos^2\theta(1 - R_\perp)^2}{(1 + R_\perp)^2} + \sin^2\theta, \tag{20}$$

$$\varepsilon_{\text{r}\parallel} = \frac{(R_\parallel + 1)\left[(R_\parallel + 1) + \sqrt{(R_\parallel + 1)^2 - (R_\parallel - 1)^2\sin^2(2\theta)}\right]}{2\cos^2\theta(R_\parallel - 1)^2}. \tag{21}$$

The equivalent complex permittivity of the MUT can be calculated using formulas (20) and (21). From the above process, it can be seen that this method does not require obtaining the thickness of the sample in advance. It is a stable broadband equivalent complex permittivity testing method. In addition, it can be seen from the above formulas that this method also does not have the multi-value problem caused by phase ambiguity.

3. Simulation analysis

In this section, EMSMs (composite materials) were first constructed and subjected to multi-angle simulation analysis under TE polarization and TM polarization using commercial electromagnetic simulation software (Ansoft HFSS). Then, the proposed method was used to invert their equivalent complex permittivity. Finally, in Section 4, the effectiveness of the method was verified by comparing it with experimental results.

The simulation model established is shown in Fig. 4. Figure 4(a) shows the simulation model of the single-layer fused silica (FS) with a thickness of 4 mm. Figure 4(b) shows the two-layer composite material (FF) consisting of an outer layer of fiber-reinforced plastic (FRP) and an inner layer of the FS; each thickness layer is 1 mm. Figure 4(c) illustrates a commonly used honeycomb sandwich structure (HSS) for radome design, comprising two outer layers of the FRP and a middle layer of regular hexagon honeycomb material (HCM). The thickness of the FRP is 1 mm and the thickness of the HCM is 2 mm. The relative complex permittivity of the FRP is $\varepsilon_{\mathrm{rf}} = 4.2 \times (1 - \mathrm{j}0.05)$ and the relative complex permittivity of the FS is $\varepsilon_{\mathrm{rs}} = 3.8 \times (1 - \mathrm{j}0.0003)$. These relative complex permittivity values were obtained through tests using a split-cylinder resonator at 10 GHz (Keysight Technologies Co. Ltd., Model: 85072A). The relative complex permittivity of the HCM is set to $\varepsilon_{\mathrm{rh}} = 4.0 \times (1 - \mathrm{j}0.06)$ in the simulation.

By setting the master-slave boundary and Floquet port to simulate the test environment, the scattering parameters of the MUT are obtained. Meanwhile, to match the test scenarios in Figs. 3(b) and 3(d), ideal electrical boundaries were set on the F_0 and F_1 planes to simulate the metal plate. The simulation frequency range was set to 8–12 GHz, and simulations and inversion calculations were performed for incident angles of 20°, 30° and 40° under both TE and TM polarizations.

The relative permittivity of the FS calculated based on simulation data is shown in Fig. 5. It can be seen that the relative permittivity of the FS remains around the preset value of 3.80. Its relative permittivity does not change with incident polarization and incident angle. This is because the FS is an isotropic material, and its relative permittivity is stable under different incident polarizations and angles.

The equivalent complex permittivity of the FF is shown in Fig. 6. Under two polarizations of incidence, the equivalent relative permittivity of the FF is between 4.00 and 4.05, and the equivalent loss tangent is between 0.04 and 0.06. The equivalent complex permittivity of the FF varies slightly with the change of incident angle, mainly because both the FRP and FS are isotropic materials, and the FF composed of the two is less sensitive to changes in incident angle.

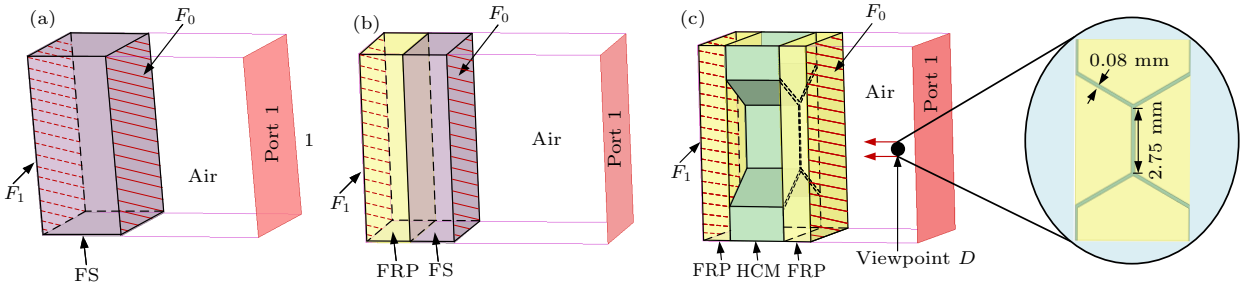


Fig. 4. Simulation model diagram. (a) FS. (b) FF. (c) HSS.

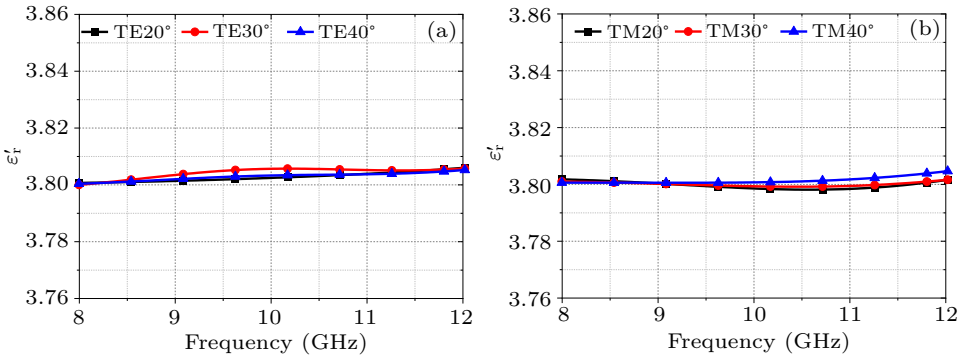


Fig. 5. Simulation results of the relative permittivity of the FS. (a) TE polarization. (b) TM polarization.

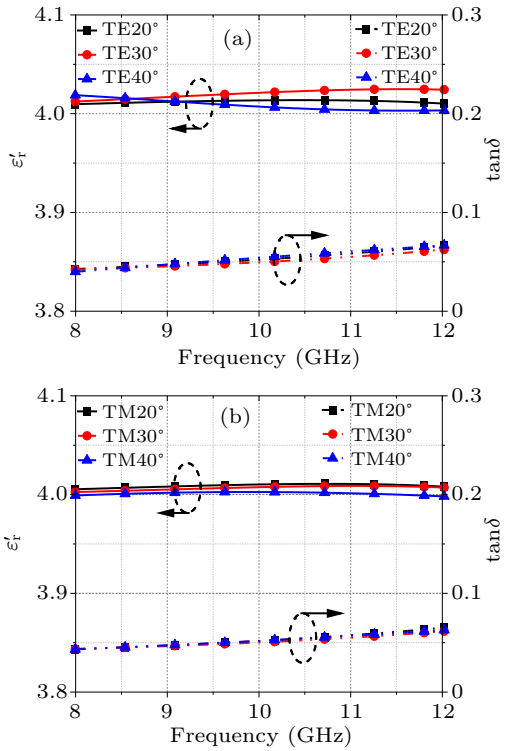


Fig. 6. Simulation results of the equivalent complex permittivity of the FF. (a) TE polarization. (b) TM polarization.

The equivalent complex permittivity of the HSS is shown in Fig. 7. Under two polarizations of incidence, the equivalent relative permittivity and the equivalent loss tangent both increase with the increase of incident angle, and this phenomenon is more significant under TM polarization. In addition, they all decrease with increasing testing frequency.

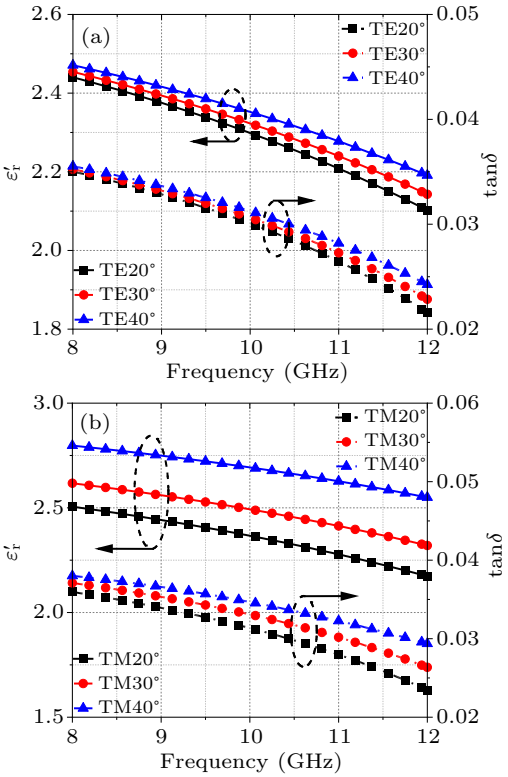


Fig. 7. Simulation results of the equivalent complex permittivity of the HSS. (a) TE polarization. (b) TM polarization.

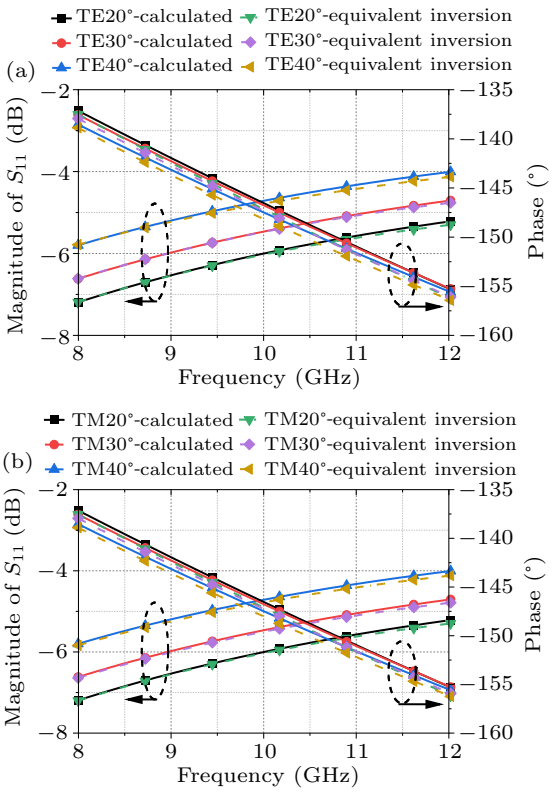


Fig. 8. Calculation results of the reflection coefficient S_{11} of multi-layer structure and single-layer equivalent medium backed by air. (a) TE polarization. (b) TM polarization.

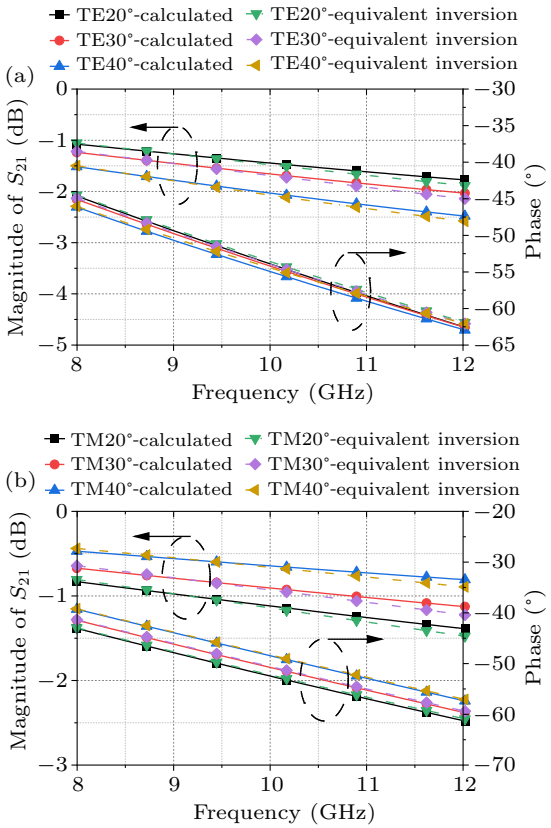


Fig. 9. Calculation results of the transmission coefficient S_{21} of multi-layer structure and single-layer equivalent medium backed by air. (a) TE polarization. (b) TM polarization.

In simulation modeling, a multi-layer composite structure can be replaced by a single-layer equivalent medium with the

same thickness to simplify the design process. To verify the feasibility of this idea, the relative complex permittivity of each layer in the FF was used to calculate its reflection coefficient S_{11} and transmission coefficient S_{21} towards air. Similarly, the method extracts the equivalent complex permittivity to simulate a single-layer medium. Its reflection coefficient and transmission coefficient against the air are calculated through equivalent inversion. Both comparison results are shown in Figs. 8 and 9. Both calculation results have good consistency under different incident polarizations and incident angles. This indicates that this method is feasible for equivalent single-layer modeling of complex structures.

4. Experimental verification

4.1. Testing system and results

Figure 10 shows the measurement system established based on the proposed method, where a vector network analyzer (VNA) 3672B from Ceyear Technologies Co. Ltd. is used. Antenna 1 and antenna 2 are both dielectric lens horn antennas, which can form the quasi-plane wave at the MUT. The working frequency of both antennas is 8–12 GHz. Their average 3-dB focal spot size is 46.6 mm. The two antennas are mounted on a circular rail to enable the adjustment of the incidence and reception angles of EM waves. Figure 11 shows several MUTs, including the FS (4 mm), FF (the thickness and composition are consistent with Section 3), and HSS (the thickness is consistent with Section 3). The testing process of each MUT was carried out according to the four steps in Fig. 3. All MUTs have dimensions of 300×300 mm.

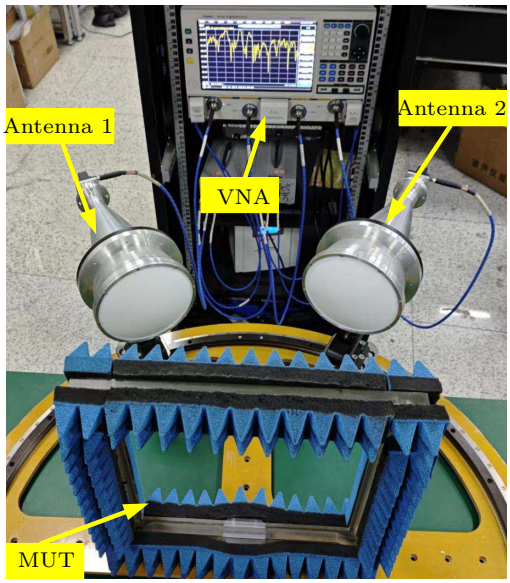


Fig. 10. Measurement system.

It is worth noting that since the reflection coefficient test is conducted under oblique incidence, the possible impact of the Brewster angle must be considered.[24] When EM waves are obliquely incident at the Brewster angle, all horizontally polarized components in the reflected wave will be transmitted, which can cause significant errors in the calculation of the complex permittivity. Therefore, it is necessary, as much as possible, to avoid testing from this angle.

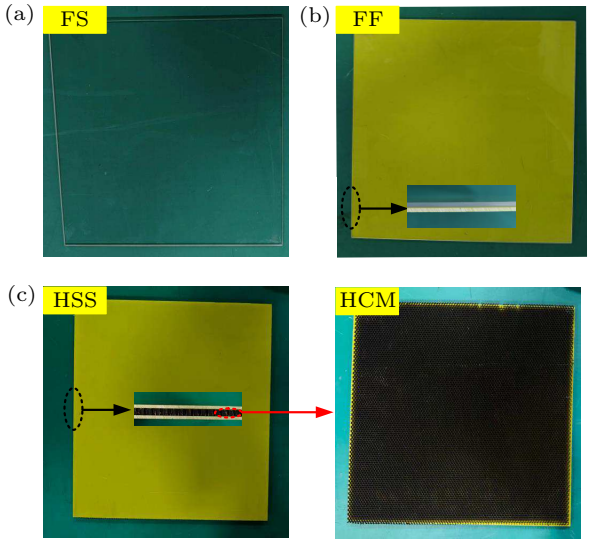


Fig. 11. Sample to be tested. (a) FS. (b) FF. (c) HSS.

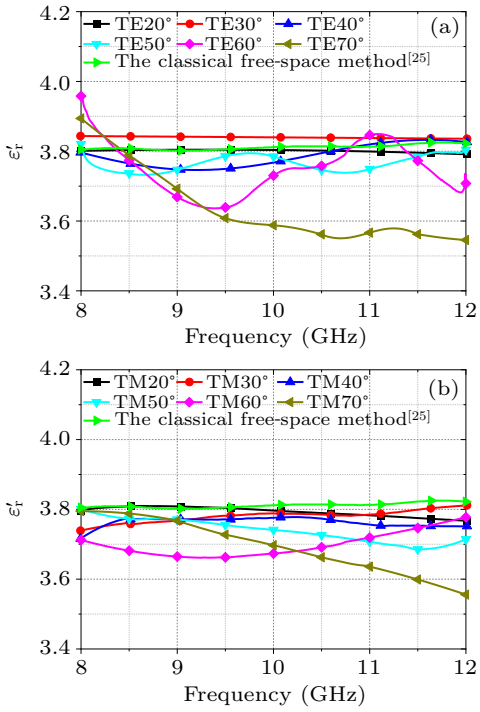


Fig. 12. Test results of the relative permittivity of the FS. (a) TE polarization. (b) TM polarization.

First, to verify the effectiveness and accuracy of the method, the FS results under different polarizations and angles were compared with the results of the classical free-space method (under vertical incidence).[25] The comparison results are shown in Fig. 12. In addition, the size of the MUT under free-space testing should be greater than three times the focal spot size to reduce the significant testing error caused by edge diffraction of the MUT.[26] In the test under oblique incidence, as the incidence angle increases, the projection size of the FS

in the vertical plane of the antenna beam propagation direction continuously decreases. Therefore, in Fig. 12, test results with incident angles of 20°, 30°, 40°, 50°, 60° and 70° are provided under TE polarization and TM polarization incidence, respectively, to determine the impact of incident angles on test accuracy.

From Fig. 12, when the incident angle is less than 60°, the equivalent relative permittivity of the FS remains stable at around 3.8, and has good consistency with the test results of the classical free-space method. As the incident angle increases, the deviation between the equivalent relative permittivity of the FS and the test value of the classical free-space method also increases. To quantify these results, the differences between the test results under the multi-angle and the classical free-space method were calculated, as shown in Tables 1 and 2.

From the results in Tables 1 and 2, the deviation is generally within 2% when the incident angle is less than 40°. When the incident angle increases to 60°, the deviation is around 4%. When the incident angle is 70°, the maximum deviation reaches 7.22%. This is because when the incident angle is 70°, the effective projection size of the FS is $300 \times \cos(70°) \approx 102.61$ mm, and at this time the edge diffraction effect produces significant testing errors. Therefore, as the incident angle increases, the accuracy of the test will decrease to some extent. To achieve good testing accuracy at large incident angles, it is necessary to increase the size of the MUT during the testing process.

Table 1. Measurement results of the FS under TE polarization.

Frequency (GHz)	Method[25]	Proposed method (TE polarization)						Deviations					
	ε_r'	ε_r'						$\Delta\varepsilon_r'$ (%)					
		20°	30°	40°	50°	60°	70°	20°	30°	40°	50°	60°	70°
8.0	3.805	3.801	3.844	3.796	3.821	3.958	3.894	0.11	1.02	0.24	0.42	4.02	2.34
8.5	3.808	3.803	3.842	3.765	3.737	3.774	3.788	0.13	0.89	1.13	1.86	0.89	0.53
9.0	3.802	3.804	3.842	3.728	3.747	3.669	3.692	0.05	1.05	1.95	1.45	3.50	2.89
9.5	3.805	3.804	3.841	3.750	3.786	3.639	3.608	0.03	0.95	1.45	0.50	4.36	5.18
10.0	3.812	3.804	3.840	3.767	3.785	3.730	3.588	0.21	0.73	1.18	0.71	2.15	5.88
10.5	3.814	3.802	3.839	3.795	3.746	3.758	3.562	0.21	0.66	0.50	1.78	1.47	6.61
11.0	3.813	3.799	3.838	3.820	3.749	3.846	3.567	0.37	0.66	0.18	1.68	0.87	6.45
11.5	3.822	3.796	3.837	3.832	3.784	3.773	3.562	0.68	0.39	0.26	0.99	1.28	6.80
12.0	3.822	3.791	3.836	3.827	3.804	3.708	3.546	0.81	0.37	0.13	0.47	2.98	7.22

Table 2. Measurement results of the FS under TM polarization.

Frequency (GHz)	Method[25]	Proposed method (TM polarization)						Deviations					
	ε_r'	ε_r'						$\Delta\varepsilon_r'$ (%)					
		20°	30°	40°	50°	60°	70°	20°	30°	40°	50°	60°	70°
8.0	3.805	3.797	3.740	3.716	3.801	3.712	3.795	0.21	1.71	2.34	0.11	2.44	0.26
8.5	3.808	3.809	3.759	3.772	3.773	3.682	3.788	0.03	1.29	0.95	0.92	3.31	0.53
9.0	3.802	3.808	3.767	3.772	3.771	3.665	3.768	0.16	0.92	0.79	0.82	3.60	0.89
9.5	3.805	3.804	3.782	3.771	3.755	3.662	3.728	0.03	0.60	0.89	1.31	3.76	2.02
10.0	3.812	3.796	3.788	3.776	3.741	3.673	3.697	0.42	0.63	0.94	1.86	3.65	3.02
10.5	3.814	3.789	3.785	3.773	3.726	3.692	3.663	0.66	0.76	1.07	2.31	3.20	3.96
11.0	3.813	3.783	3.785	3.756	3.707	3.719	3.636	0.79	0.73	1.49	2.78	2.47	4.64
11.5	3.822	3.775	3.799	3.753	3.686	3.747	3.599	1.23	0.60	1.81	3.56	1.96	5.83
12.0	3.822	3.767	3.811	3.751	3.714	3.777	3.556	1.44	0.29	1.86	2.83	1.18	6.96

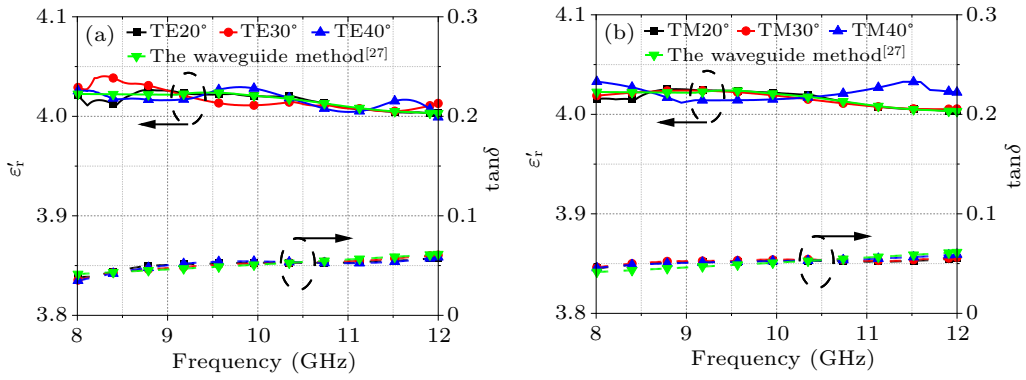


Fig. 13. Test results of equivalent complex permittivity of the FF. (a) TE polarization. (b) TM polarization.

Subsequently, the FF was tested under different incident polarizations and angles. At the same time, the test results were compared with those obtained using the waveguide method (under vertical incidence).[27] The test results are shown in Fig. 13. The equivalent relative permittivity remains stable between 4.00 and 4.05, and the equivalent loss tangent remains stable between 0.04 and 0.06. The test results show good consistency and stability compared to Fig. 6, indicating that this method has high testing accuracy.

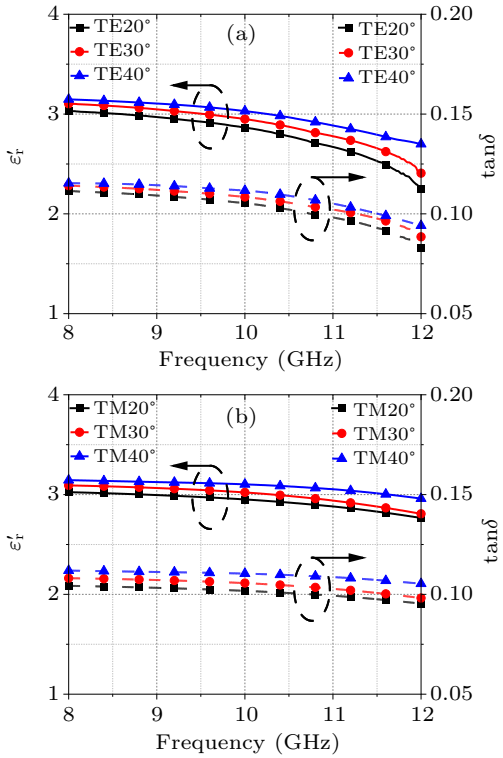


Fig. 14. Test results of equivalent complex permittivity of the HSS. (a) TE polarization. (b) TM polarization.

Finally, the HSS was tested under different incident polarizations and angles, and the test results are shown in Fig. 14. The equivalent relative permittivity and equivalent loss tangent increase with the increase of incident angle under TE polarization and TM polarization. They all decrease with increasing frequency. This phenomenon is consistent with the trend shown in Fig. 7. However, due to the inability to obtain the complex permittivity of the base material for the HCM, there are numerical differences between the simulation results in Fig. 7 and the test results in Fig. 14.

4.2. Error analysis

From the previous analysis, the minimum size of the MUT should meet the requirement of three times the focal spot diameter, which is a prerequisite for maintaining good testing accuracy. In addition, according to the testing physical model and theoretical calculation process of this method, the main error sources in complex permittivity testing are listed as follows. 1) The error caused by the uncertainty in measuring the amplitude of reflection coefficients under four different reflection states. 2) The error caused by the uncertainty in measuring the phase of reflection coefficients under four different reflection states. 3) The error caused by the uncertainty of the angle due to adjusting the incident and receiving angles of EM waves when the test antennas move on a circular arc track.

The performance of the VNA determines the uncertainty of the amplitude and phase measurements of the reflection coefficient during testing. The amplitude and phase measurement uncertainties of 3672B from Ceyear Technologies Co. Ltd. are less than 0.004 and 0.05°, respectively. Therefore, when measuring the reflection coefficient in four different reflection states, the uncertainty of the amplitude and phase measurement of the reflection coefficient is $\Delta M_i = 0.004$ and $\Delta\varphi_i = 0.05°$, respectively. Among them, $i = 1$, 2, 3 and 4 correspond to the four test states in Fig. 3.

In addition, during oblique incidence testing, it is necessary to slide the antennas to adjust the angle of incidence and reception of EM waves, which can introduce certain angle errors. In the test, this error can be minimized as much as possible by using a high-precision angle dial, and the angle error can be controlled within 1°. Therefore, the uncertainty of the angle caused by EM waves is $\Delta\theta = 1°$.

Based on the above error sources, the comprehensive error of equivalent relative permittivity testing is given by

$$|\Delta\varepsilon_r'| = \sqrt{\sum_{i=1}^{4}\left(\frac{\partial\varepsilon_r'}{\partial M_i}\cdot\Delta M_i\right)^2 + \sum_{i=1}^{4}\left(\frac{\partial\varepsilon_r'}{\partial\varphi_i}\cdot\Delta\varphi_i\right)^2 + \left(\frac{\partial\varepsilon_r'}{\partial\theta}\cdot\Delta\theta\right)^2}. \tag{22}$$

Similarly, the source of error in the equivalent loss tangent is consistent with the equivalent relative permittivity. The comprehensive error of equivalent loss tangent testing is

$$|\Delta\tan\delta| = \sqrt{\sum_{i=1}^{4}\left(\frac{\partial\tan\delta}{\partial M_i}\cdot\Delta M_i\right)^2 + \sum_{i=1}^{4}\left(\frac{\partial\tan\delta}{\partial\varphi_i}\cdot\Delta\varphi_i\right)^2 + \left(\frac{\partial\tan\delta}{\partial\theta}\cdot\Delta\theta\right)^2}. \tag{23}$$

Based on the above analysis, the test errors of the FS, FF and HSS are evaluated. The results are shown in Tables 3–5. It can be seen that the uncertainty of the equivalent relative permittivity for the FS, FF and HSS is less than 3.16%, 3.48% and 4.89%, respectively. The uncertainty of the equivalent loss tangent for the FS, FF and HSS is less than 4.09%, 4.03% and 5.82%, respectively.

Table 3. Measurement uncertainty of the equivalent complex permittivity of the FS.

Frequency (GHz)	TE polarization						TM polarization					
	$\lvert\Delta\varepsilon_r'\rvert/\varepsilon_r'$ (%)			$\lvert\Delta\tan\delta\rvert/\tan\delta$ (%)			$\lvert\Delta\varepsilon_r'\rvert/\varepsilon_r'$ (%)			$\lvert\Delta\tan\delta\rvert/\tan\delta$ (%)		
	20°	30°	40°	20°	30°	40°	20°	30°	40°	20°	30°	40°
8.0	0.94	1.53	2.14	1.35	0.52	0.81	1.00	0.91	1.92	1.18	2.18	1.41
8.5	0.80	0.97	1.51	0.80	1.33	0.84	0.98	1.19	2.85	2.23	1.54	2.86
9.0	1.12	1.11	2.42	1.38	1.83	1.12	1.07	1.37	1.79	1.27	1.32	3.81
9.5	1.54	1.52	2.17	2.31	2.25	0.78	1.29	2.03	2.21	1.43	2.75	4.09
10.0	0.92	1.51	2.53	0.81	1.27	1.77	1.01	2.27	1.26	1.36	2.92	2.71
10.5	1.05	1.05	3.16	1.35	1.53	2.01	0.97	1.68	1.05	1.01	3.19	2.82
11.0	0.84	1.49	2.62	1.56	0.71	2.79	1.87	0.99	1.55	2.34	2.70	1.83
11.5	0.85	1.88	2.14	1.15	1.55	0.80	1.13	1.33	2.48	1.87	2.47	2.07
12.0	0.93	1.50	1.57	1.37	0.79	1.11	1.39	2.01	1.81	2.35	1.84	2.59

Table 4. Measurement uncertainty of the equivalent complex permittivity of the FF.

Frequency (GHz)	TE polarization						TM polarization					
	$\lvert\Delta\varepsilon_r'\rvert/\varepsilon_r'$ (%)			$\lvert\Delta\tan\delta\rvert/\tan\delta$ (%)			$\lvert\Delta\varepsilon_r'\rvert/\varepsilon_r'$ (%)			$\lvert\Delta\tan\delta\rvert/\tan\delta$ (%)		
	20°	30°	40°	20°	30°	40°	20°	30°	40°	20°	30°	40°
8.0	0.97	1.52	2.14	1.12	0.51	0.81	1.04	0.93	1.32	0.29	2.87	1.63
8.5	2.52	0.97	2.38	3.25	1.33	0.85	1.38	2.34	2.86	1.50	2.91	1.81
9.0	0.97	1.09	1.72	2.33	1.53	1.08	0.61	1.35	1.90	1.24	1.30	2.94
9.5	0.98	1.58	1.04	2.34	1.24	1.18	2.07	2.19	2.57	2.30	1.51	3.05
10.0	1.06	1.74	2.04	1.34	2.57	1.92	2.19	2.56	3.21	2.95	3.95	2.77
10.5	1.17	1.33	2.31	1.68	0.54	1.56	1.03	1.29	1.67	3.01	2.30	4.03
11.0	0.97	1.49	1.03	2.04	1.45	2.26	1.28	1.09	1.62	3.15	1.51	2.18
11.5	0.94	1.88	2.35	0.36	0.55	2.92	1.89	1.94	1.59	1.32	1.24	2.42
12.0	0.99	1.54	3.04	2.12	1.47	3.91	1.06	1.64	3.48	1.26	2.61	2.84

Table 5. Measurement uncertainty of the equivalent complex permittivity of the HSS.

Frequency (GHz)	TE polarization						TM polarization					
	$\lvert\Delta\varepsilon_r'\rvert/\varepsilon_r'$ (%)			$\lvert\Delta\tan\delta\rvert/\tan\delta$ (%)			$\lvert\Delta\varepsilon_r'\rvert/\varepsilon_r'$ (%)			$\lvert\Delta\tan\delta\rvert/\tan\delta$ (%)		
	20°	30°	40°	20°	30°	40°	20°	30°	40°	20°	30°	40°
8.0	0.68	2.26	0.78	1.95	4.20	3.11	0.76	0.22	2.18	3.16	4.26	2.08
8.5	2.17	3.85	1.88	2.76	5.15	4.73	2.87	0.31	1.85	4.32	3.90	5.08
9.0	4.33	4.72	3.07	3.17	3.91	5.82	3.04	0.16	2.53	4.74	3.95	3.13
9.5	2.26	3.73	4.76	0.99	1.76	6.11	2.45	4.17	4.17	0.83	1.39	2.39
10.0	1.79	2.95	4.89	0.50	0.95	4.25	1.94	2.80	0.44	0.53	1.51	2.92
10.5	1.64	2.64	4.10	0.35	0.62	2.27	1.71	2.48	3.45	1.34	1.31	1.27
11.0	1.53	2.43	4.33	0.54	0.40	1.45	1.58	2.33	3.25	1.24	2.22	2.16
11.5	1.47	2.31	3.92	1.18	1.28	1.02	1.55	2.29	3.20	1.21	1.91	2.13
12.0	1.39	2.20	3.60	1.09	1.17	0.69	1.46	2.21	3.13	0.93	1.19	3.08

5. Conclusion

EMSM is a type of material that is sensitive to the polarization and incidence angle of EM waves and exhibits different scattering characteristics under oblique incidence. To effectively determine the dielectric properties of EMSM, this paper proposes a broadband inversion method for measuring the equivalent complex permittivity. This method establishes multiple equations to solve the equivalent complex permittivity of the material by conducting multi-reflection tests under oblique incidence. It is a stable calculation method that does not need to know the thickness of the sample and can avoid phase ambiguity. Simulation results show that this method can not only effectively extract the equivalent complex permittivity of EMSM under different incident polarizations and angles but also provide an alternative design for modeling and designing complex structures using equivalent single-layer dielectric materials. We have also constructed a corresponding testing system, and this method has been validated through simulation and experimentation as an effective and accurate testing method. It can provide efficient application and guidance value for the analysis of dielectric properties and complex modeling of EMSM.

Acknowledgements

This project is supported by the National Natural Science Foundation of China (Grant Nos. 62201130 and 62301134) and the Fundamental Research Funds for the Central Universities (Grant No. JZ2025HGTB0222).

References

[1] Baida F I, Boutria M, Oussaid R and Labeke D V 2011 *Phys. Rev. B* **84** 035107

[2] Poyanco J M, Pizarro F and Rajo-Iglesias E 2024 *IEEE Trans. Antennas Propag.* **72** 5343

[3] Liao Y and Chen J N 2024 *Chin. Phys. B* **33** 078401

[4] Wang Y, Han T C, Liang D F and Deng L J 2023 *Chin. Phys. Lett.* **40** 104101

[5] Zhang J M, He D L, Wang G W, Wang P, Qiao L, Wang T and Li F S 2019 *Chin. Phys. B* **28** 058401

[6] Hasar U C, Muratoglu A, Bute M, Barroso J J and Ertugrul M 2017 *IEEE Trans. Microw. Theory Techn.* **65** 1488

[7] Trang F, Rogalla H and Popovi Z 2015 *IEEE Trans. Appl. Supercond.* **25** 1800107

[8] Feng T Q, Yu C Y, Li N and Shi Y 2023 *Chin. Phys. B* **32** 030101

[9] Li L, Chen X M, Ni L and Fu M S 2007 *Appl. Phys. Lett.* **91** 092906

[10] Wang J S, *et al.* 2023 *Chin. Phys. Lett.* **40** 118101

[11] Chen H Y, Shen R B, Li F X, He Q T, Li G Y, Lu H P, Weng X L, Xie J L, Zhang G R and Deng L J 2021 *Appl. Phys. B* **127** 84

[12] Rashidian A, Shafai L, Klymyshyn D and Shafai C 2017 *IEEE Antennas Wireless Propag. Lett.* **16** 2630

[13] Xiang Z, Wu J, Qi C and Hu X 2020 *IEEE Trans. Instrum. Meas.* **69** 2139

[14] Barroso J J and Hasar U C 2012 *J. Infr. Millim. THz Waves* **33** 237

[15] Rebouas J A and P A Brando 2022 *Phys. Rev. A* **106** 043503

[16] Ozturk G, Hasar U C, Bute M and Ertugrul M 2021 *IEEE Trans. Antennas Propag.* **69** 918

[17] Li Z, Aydin K and Ozbay E 2009 *Phys. Rev. E* **79** 026610

[18] Hasar U C, Buldu G, Kaya Y and Ozturk G 2018 *IEEE Trans. Microw. Theory Techn.* **66** 3734

[19] Chen X, Grzegorczyk T M, Wu B I, Pacheco J and Kong J A 2004 *Phys. Rev. E* **70** 016608

[20] Shi Y, Hao T, Li L and Liang C H 2016 *Microw. Opt. Technol. Lett.* **58** 647

[21] Luukkonen O, Maslovski S I and Tretyakov S A 2011 *IEEE Antennas Wireless Propag. Lett.* **10** 1295

[22] Li L, Hu H, Tang P, Li R, Chen B and He Z 2018 *IEEE Antennas Wireless Propag. Lett.* **17** 575

[23] Zhang L, Lu H, Zhou P, Xie J and Deng L 2015 *IEEE Trans. Magn.* **51** 7100604

[24] Wang Z S, Sang T, Wang L, Zhu J T, Wu Y G and Chen L Y 2006 *Appl. Phys. Lett.* **88** 251115

[25] Boughriet A H, Legrand C and Chapoton A 1997 *IEEE Trans. Microw. Theory Techn.* **45** 52

[26] Ghodgaonkar D K, Varadan V V and Varadan V K 1989 *IEEE Trans. Instrum. Meas.* **38** 789

[27] Jiang C and Yang C F 1995 *Microw. Opt. Technol. Lett.* **9** 41